Localized Protection of Radial DC Microgrids with High Penetration of Constant Power Loads

Bayati, Navid; Baghaee, Hamid Reza; Hajizadeh, Amin; N. Soltani, Mohsen

Published in:
I E E E Systems Journal

DOI (link to publication from Publisher):
10.1109/JSYST.2020.2998059

Publication date:
2021

Document Version
Accepted author manuscript, peer reviewed version

Localized Protection of Radial DC Microgrids With High Penetration of Constant Power Loads

Navid Bayati, Hamid Reza Baghaee, *Member, IEEE*, Amin Hajizadeh, *Senior Member, IEEE*, and Mohsen Soltani, *Senior Member, IEEE*

***Abstract*—This article proposes a localized protection scheme for dc microgrids with radial configuration under the impact of constant power loads (CPLs) to determine the location of faults accurately. The proposed fault location scheme is primarily designed for fault location of CPLs in dc microgrids. First, a local protection relay for CPL is designed based on the transient behavior of the current and voltage in the main distribution line. Then, the estimation of the fault resistance is formulated based on the power sharing in the system to improve the accuracy of the protection system. To realize a robust protection scheme considering the variation of fault resistance, a fault resistance estimation procedure is employed to design a system that locates both low- and high-impedance faults. Finally, the effectiveness of the proposed strategy is evaluated based on offline digital time-domain simulations in Digsilent PowerFactory software environment and experimentally verified by implementing on a laboratory scale hardware setup. The obtained simulation and experimental test results, and comparison with other methods prove that the proposed scheme is immune against these disturbances and can efficiently and reliably estimate the location and resistance of faults with high accuracy and acceptable error margin.**

***Index Terms*—Constant power loads (CPL), dc microgrid, fault detection, fault location, protection.**

Nomenclature

AC	Alternating current.
CPL	Constant power loads.
DC	Direct current.
DER	Distributed energy resources.
FC	Fuel cells.
HIF	High-impedance fault.
INR	Incremental negative resistance.
LV	Low voltage.
PMU	Phasor measurement unit.
PV	Photovoltaic.
WT	Wind turbine.
V	Voltage.
I	Current.
P	Power.
R	Resistance.
R_{seen}	Measured resistance by relay.
R_{fault}	Fault resistance.
V_{CPL}	CPL voltage.
I_{CPL}	CPL current.
V_F	Fault voltage.
I_F	Fault current.
V_C	DC-link capacitor voltage.
V_o	Initial voltage during a fault or the prefault values.
I_o	Initial current during a fault or the prefault values.
C	Capacitance.
P_{CPL}	CPL power.
P_{cable}	Power losses by cable.
P_{fault}	Power of fault resistance.
P_{relay}	Measured power by relay.
R_{cable}	Cable resistance.
L_C	Inductance of cable per km.
R_C	Resistance of cable per km.
$I_{\text{fault(tn)}}$	Sampled fault current.
Δt	Sampling interval.
$P_{\text{relay(tn)}}$	Sampled fault power.

Manuscript received March 27, 2020; revised May 7, 2020 and May 23, 2020; accepted May 24, 2020. *(Corresponding author: Navid Bayati.)*

Navid Bayati, Amin Hajizadeh, and Mohsen Soltani are with the Department of Energy Technology, Aalborg University, Aalborg 9100, Denmark (e-mail: nab@et.aau.dk; aha@et.aau.dk; sms@et.aau.dk).

Hamid Reza Baghaee is with the Department of Electrical Engineering, Amirkabir University of Technology, Tehran 15914, Iran (e-mail: hrbaghaee@aut.ac.ir).

Digital Object Identifier 10.1109/JSYST.2020.2998059

I. Introduction

THE growing penetration of dc renewable/nonrenewable DERs such as WT, PV, and FCs and loads have motivated an increasing interest in dc microgrids [1], [2]. DC microgrids have some inherent advantages over ac systems since no reactive power, frequency, and impedance losses are present in dc microgrids [3].

The primary concern in the protection problem of dc microgrids is how to design a feasible, fast, and accurate protection scheme to locate and isolate the faulty section. In the last few years, several types of research have presented dc microgrid protection, mainly using overcurrent, distance, and differential relays. In [4], a hybrid passive overcurrent relay has been investigated for LV dc grids based on detecting the dc faults. It uses overcurrent function and the wavelet transform. In this strategy, the relays are localized; however, they cannot locate the faults, and thus, this method cannot be used for load protection. To handle this dilemma, traveling wave-based distance protection has been used in [5] for dc microgrids using the wave shape and polarity of these waves to locate faults. Another technique that is implemented in dc microgrid protection is differential protection [6], [7]. In [6], high-speed differential protection has been used

for dc systems, which can detect the fault within 2 ms. This method uses the natural behavior of the dc current to decrease the fault detection time. But, the problem of the differential relays is that they are not localized and need the information of two ends of the lines, and they are vulnerable to noise.

On the other hand, one of the main loads of dc microgrids is CPL. In a dc microgrid, the CPL (also known as an active load) enables a specific behavior at the load side. Dissimilar to passive loads, the CPLs (for instance, constant power energy storage, dc motor, etc.) consume a constant power regardless of the voltage. Also, the behavior of a converter-based load is defined by the control system. For example, for a point of load, the load converter can be in voltage control mode to keep the voltage in a prespecified constant value. Therefore, these types of loads can be regarded as a CPL. The application of CPLs can be found in different systems, such as microgrids [7] and maritime [9]. The INR of CPLs affects the protection system design of whole systems so that the system can be damped poorly by the INR during instability. During the fault, the voltage of the system will drop. Hence, the INR impact of the CPL accelerates the increasing trend of fault current, and consequently, it causes a wrong performance in the dc microgrid protection scheme. Protection issues should be noticed to enhance the reliability of a dc microgrid, mainly when the system includes CPLs. The mentioned issue induced by CPL has not been studied extensively, up to now. The fault location in CPLs is the focus of this article since a transient and comprehensive model of a dc microgrid includes different components, and the CPLs are modeled.

Meanwhile, the behavior of CPLs must be taken into account when analyzing the protection of the microgrid with CPLs. Besides, many articles have focused only on single-bus systems where DERs and loads are connected at one bus. Also, an LV dc microgrid has been built in India [10], in which the DERs are connected to one bus, and loads are connected to other buses. Then, the voltages of different locations are different, and the current depends on the CPLs. Hence, the current signal behavior gets worse during the faults, and protection schemes can be mis-coordinated in this situation. The fault location schemes currently implemented in most dc microgrids uses the current signals of both ends of lines or components by communication links. This type of fault locating system for radial dc microgrids are discussed in [11]. Generally, the communication-based fault location methods increase the cost of the protection scheme. There is also the probability of noise and communication failure.

In this article, a new local fast fault location and resistance estimation strategy are proposed. A transient-based relay during the fault is exploited for estimating fault resistance using a power-sharing approach in the lines equipped with CPLs. Due to the different characteristics of CPLs, and their growing penetration, the focus of this article is the HIF location of dc microgrids in the presence of CPLs. The proposed fault location strategy considers the transient behavior of the fault current, and prefault data to find the exact location of the faulty CPLs and the lines connected to CPLs. This method is quite accurate, cost-effective, and fast due to its localized nature. Also, by calculating unknown fault resistance during the transient fault period, a fast fault location strategy is proposed using a noniterative algorithm. The proposed localized dc microgrid fault location strategy works effectively during dc faults by considering different values of fault resistance. The transient and localized approaches are employed to remove the communication time delay, reduce the implementation costs, and increase reliability, accuracy, and speed of protection scheme of dc microgrids with high penetration of CPLs. Because of the scalability feature of the proposed strategy, for more complex dc systems, the computational burden of the proposed algorithm on the transient current will be higher, where the basic scheme will remain the same. Because one measurement is required for the proposed localized fault location scheme, the fault location is done by comparing the slopes of the fault currents and prefault data. Fault distance is calculated by the ratio of the slope reduction trend in line. The performance of the proposed fault location scheme is evaluated for HIF with different scenarios and loads in a scaled-down hardware setup in the laboratory.

To realize the concepts mentioned above, this article is decomposed into the following steps. The related existing works are described and compared in Section II. Then, first, an accurate model of CPLs in dc microgrid is introduced in Section III to analyze the transient behavior of CPLs and the system during the fault. Afterward, the fault location scheme is proposed in Section IV, which estimates the fault resistance during the fault by using the power-sharing in the power system. Then, based on the transient behavior of the current and voltage signals in the relay location, fault detection and location are introduced. Finally, the effectiveness, accuracy, authenticity, and efficiency of the proposed protection and fault location strategy and the presented fault resistance estimation is proved using offline digital time-domain simulations and experimentally verified by experimental testbed in the lab in Sections V and VI, respectively. Then, discussions and comparisons are presented in Section VII. Finally, conclusions are stated in Section VIII.

II. Previous and Related Works

Due to the providing electricity for loads or RESs at the end of lines in radial dc microgrids, the fault locating of radial dc microgrids is still a challenging task. In [12], a fault location strategy has been presented for locating the low impedance faults in radial dc microgrids, by using frequency spectrum components of fault generated traveling waves. Moreover, Karmacharya and Gokaraju [13] and Jiang *et al.* [14] suggest a fault location method for locating fault in PV and terminal in a dc microgrid, respectively. However, the drawback of these methods is that they cannot locate HIFs in a dc microgrid and also did not consider the impact of CPLs. A PMU-based fault location method is suggested in [15] to locate HIFs; however, high dependence on communication links and PMUs increases the cost and noise of this method. In [16], the HIF location for HVdc systems is presented without using communication links, but it only can be implemented in transmission links between terminals. It cannot consider the dynamic of loads. Also, load protection has been proposed in [16] for a radial LV dc microgrid using negative sequence superimposed directional

TABLE I
SUMMARIZING THE EXISTING FAULT LOCATION METHODS

Communication infrastructure	HIF	Method	Technique	Application	Type of load	Cost
Local	Not considered	[13]	Wavelet and artificial neural network	Ungrounded PV system	Without DC loads	Low
Local	Not considered	[20]	Circuit analysis	VSC-Based DC Network Cables	Not considered	Low
Local	Not considered	[21]	Using Active Impedance Estimation	DC Marine power systems	Not considered	High
Local	Not considered	[22]	Traveling-wave based	DC Microgrid	Not considered	High
Local	Considered	[16]	Harmonic analysis	HVDC	Not considered	Low
Communication-based	Considered	[12]	Traveling-Wave-Based Methodology	Multiterminal DC Systems	Not considered	Very High
Communication-based	Considered	[15]	Probabilistic analysis	Radial DC systems	Resistive load	High
Communication-based	Considered	[23]	Traveling-wave	Multi-terminal DC networks	Not considered	High
Communication-based	Considered	[24]	Wavelet modulus maxima	DC systems with electric vehicle charging load	Not considered	Low
Communication-based	Considered	[26]	Differential fault location	Low-Voltage DC Line	Considered	High
Communication-based	Considered	[27]	Analyzing the behavior of DC fault voltage	DC distribution networks	Considered	High
Communication-based	Not considered	[14]	Analyzed fault characteristic	DC Lines connected to terminals	Not considered	High
Communication-based	Not considered	[25]	Multi-Criterion System and neural network	DC microgrids systems	Not considered	High

protection for adjustment of the settings of protection devices. Other strategies for radial systems have been reported in [18]–[20] based on adaptive protection for radial microgrids. In dc microgrid systems, most of the load branches are radial, and other sections may have a loop feeder; however, the loops are operated as an open circuit by normally open switches which are closed during the faults. Thus, preserving the radial operation of dc microgrids, the fault location scheme of loads are typically designed. The fault location schemes can be categorized as local or communication-based methods.

A. Local Methods

The fault location of dc marine systems is suggested in [21] by using active impedance estimation. In this method, a short duration current is injected into the system, and the measured value of transient response is used to determine the active impedance. The local traveling-wave method in [22] uses the response of an injected current at one point to locate the fault. However, these methods require costly additional equipment to inject current and measure the response of it by a high sampling rate.

B. Communication-Based Methods

The traveling-wave-based fault location method is presented in [23], which records the first arrival time of current after a fault at all terminals of a dc system, and the graph theory is used to extract the feature of current to locate the fault. In [24], the fault location of a dc system equipped with electric vehicle charging loads is suggested. It uses a signal processing method, wavelet transform, to estimate the location of the fault. The differential based fault location method for a dc microgrid by using the multicriterion system and neural network is presented in [25]. This method requires a communication link between two relays at both sides of each line segment, which increases the cost, noise, and failure probability. In [26], a current differential fault location method for dc lines is suggested to determine the line fault zone. The attenuation characteristics of the dc line current is used to develop this technique. Based on analyzing the behavior of dc fault voltage, the relationship between the fault location and voltage is determined in [27], and the pseudo-dual-root problem is solved for this aim.

Typically, eliminating the communication link in designing a protection system has several advantages such as, reducing cost and noise and avoiding the synchronization problem between measurement units in high length line systems. Therefore, local fault location schemes are more reliable as reducing the causes of the error by different equipment and synchronization time at both ends of the line. Consequently, the local fault location methods are more practical and accurate in fault location. The comparison of related works is summarized in Table I.

III. BEHAVIOR OF CPLS DURING THE FAULT

The converter, along with its controller, is one of the main parts of dc microgrids. In these systems, the majority of loads, such as loads with a regulator and electronic loads, are tightly controlled. These converters behave as a CPL. Due to the constant consumption of power, the behavior of V and I can be described by, as shown in Fig. 1

$$P = V * I = \text{constant}. \tag{1}$$

This behavior of CPLs makes a problem for the protection of dc microgrids so that during the fault, the voltage of the

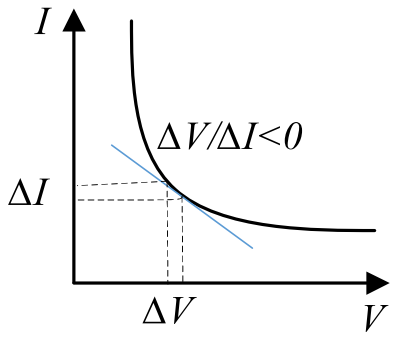

Fig. 1. *V–I* curve of CPLs.

system will be dropped, and CPLs consume more current for maintaining the constant power for the load. It accelerates the fault current rising [28]. As shown in Fig. 1, the CPLs behave as negative resistance, which is known as INR. Based on (1), the relation of current and voltage is given by

$$R = \frac{\Delta V_{\mathrm{CPL}}}{\Delta I_{\mathrm{CPL}}} = -\frac{P}{I^2}. \tag{2}$$

Due to the behavior of CPLs, the value of *R* is assigned by a negative sign, and it acts as positive feedback. This means that, although in CPLs, the instantaneous value of impedance is positive, the INR is always negative. Therefore, the current through a CPL increases when the voltage across it decreases. This has influences on the impedance-based methods such as distance relay protection because the relay senses lower impedance, and the calculated distance will be higher. For instance, a simple radial branch is shown in Fig. 2. If a distance relay installs in the bus *A*, and a fault occur between *C* and *D*, the resistance that is seen by relay will be

$$R_{\mathrm{Seen}} = R_{AB} + R_{BC} + R_{CF} + R_{\mathrm{fault}} \tag{3}$$

$$R_{\mathrm{Seen}} = \frac{V_{AB}}{I_{AB}} + \frac{V_{BC}}{I_{BC}} + \frac{V_{CF}}{I_{CF}} + \frac{V_F}{I_F} \tag{4}$$

$$I_{AB} = I_{\mathrm{CPL}} + I_{BC}. \tag{5}$$

According to (4), if a line equipped by CPLs, during the fault and voltage drop, the load current will be increased, and based on the (5), it will be decreased the fault current that flows in the main distribution line. Thus, the observed resistance by the distance relay will be increased. Therefore, the distance relay and other local protection methods cannot locate the accurate place of the fault. Thus, a specific protection system is essential for microgrids with high penetration of CPLs.

Besides, during the fault, the voltage of the system will decrease to a lower value, which depends on the amount of fault resistance. Also, CPLs behave as negative feedback during fault; then, the effect of the negative feedback of CPL and voltage drop causes a high rise of fault current, as shown in Fig. 3. Therefore, it leads to a considerable increase in fault current magnitude in a short time, which represents a threat to the stability and operation of different components in dc microgrid. Essentially, fault current in dc microgrids has three different stages. The first stage of the fault current rising in the dc microgrids is capacitor discharging. The second stage is diode flywheel, and then the steady-state or the grid current feeding stage. The proposed method only measures the values of current and voltage signals in the capacitor discharge stage. As shown in Fig. 3, this stage occurs during the dc-link capacitor-discharge, which is described by [29]

$$V_C = \frac{V_0\omega_0}{\omega}e^{-\alpha t}\sin(\omega t + \beta) - \frac{I_0}{\omega C}e^{-\alpha t}\sin\omega t \tag{6}$$

where $= R/2L, \omega = \sqrt{1/LC - \alpha^2}\,, \omega_0 = \sqrt{\alpha^2 + \omega^2}$, and $\beta = \arctan(\omega/\alpha)$. Then, a CPL can behave as a current source during the fault, as shown in Fig. 4. A function of voltage calculates the value of the current source. Therefore, during the fault and the first stage of fault rising, the value of current can be obtained by

$$f(V_{\mathrm{CPL}}) = I_{\mathrm{CPL}} = \frac{P_{\mathrm{CPL}}}{V_{\mathrm{CPL}}} \tag{7}$$

where the value of P_{CPL} is constant, and the value of V_{CPL} is variable. Then, by using (8), the value of the current is calculated as a time-variant equation

$$I_{\mathrm{CPL}} = \frac{P_{\mathrm{CPL}}e^{\alpha t}\omega}{V_0\omega_0\sin(\omega t + \beta) - \frac{I_0}{C}\sin(\omega t)}. \tag{8}$$

IV. Proposed Protection Scheme

In this section, a protection scheme is proposed for radial dc microgrids with high penetration of CPLs. The dc microgrid consists of PV, WT, BESS, and some CPLs and the proposed protection system components such as a relay, measurement, and circuit breakers. The recommended method estimates the fault resistance and location only by using a localized relay and, it provides the value of fault resistance by power-sharing, and the location of fault by using transient behavior of voltage and current in the relay place, and because it does not depend to communication links, the noise and delay and other communication latencies and uncertainties cannot impact on this protection system. The details of the proposed method are presented in the next sections.

A. Fault Resistance Estimation Technique

In a dc microgrid, during the fault, the current of the system will be increased immediately, and the rate of rising and the value of fault current depend on the fault resistance. Also, the fault location techniques need the value of fault resistance to estimate the exact location of faults. The first stage of the proposed method is the estimation of fault resistance. During the fault, the power-flow of the main distribution line will divide into several parts, namely power losses, CPLs and power consumption of fault resistance as

$$P_{\mathrm{relay}} = P_{\mathrm{cable}} + P_{\mathrm{CPLs}} + P_{\mathrm{fault}}. \tag{9}$$

On the other hand, the value of the power of cables and fault is unknown, and the value of power consumption of CPLs is known because they consume a constant value. The value of P_{relay} can measure by measurement in the relay place. So, this equation

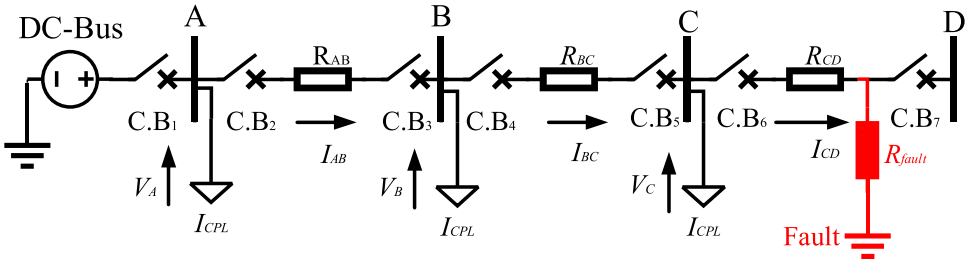

Fig. 2. Radial branch equipped with CPLs.

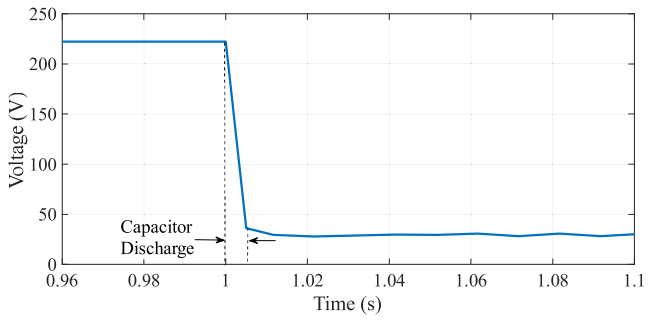

Fig. 3. Capacitor discharge in the dc microgrid.

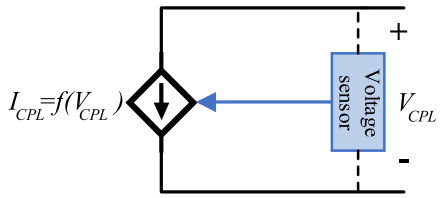

Fig. 4. Model of CPL during capacitor discharge.

has two variables, P_{fault} and P_{cable}; thus, (9) is expanded to a quadratic equation in terms of fault current as

$$P_{\text{relay}} = P_{\text{CPLs}} + R_{\text{cable}}\frac{L_C}{R_C}\frac{dI_{\text{fault}}}{dt}I_{\text{fault}} + (R_{\text{fault}} + R_{\text{cable}})I_{\text{fault}}^2 \tag{10}$$

where the value of I_{fault} measured by measurements at the relay place; however, because the fault current in the place of the relay is different from the fault current in the faulty place. Therefore, to increase the accuracy, the fault current at the faulted node is the difference of measured and load currents. The fault current in the mentioned system has a rising trend, and the relay measures the power and current at different times. The values of power in terms of fault current are written as follows:

$$\begin{aligned} P_{\text{relay}(t1)} &= A + BI_{\text{fault}(t1)} + CI_{\text{fault}(t1)}^2 \\ P_{\text{relay}(t2)} &= A + BI_{\text{fault}(t2)} + CI_{\text{fault}(t2)}^2 \\ &\vdots \\ P_{\text{relay}(\text{tn})} &= A + BI_{\text{fault}(\text{tn})} + CI_{\text{fault}(\text{tn})}^2 \end{aligned} \tag{11}$$

where the values of *A*, *B*, and *C* are given by

$$A = P_{\text{CPLs}}, B = R_{\text{cable}}\frac{L_C}{R_C}\frac{dI_{\text{fault}}}{dt}, C = R_{\text{fault}} + R_{\text{cable}} \tag{12}$$

where $I_{\text{fault}(t1)}, I_{\text{fault}(t2)}, \ldots, I_{\text{fault}(\text{tn})}$ are the sampled fault currents, and $\Delta t = t_2 - t_1$ is the sampling interval, and $P_{\text{relay}(t1)}, P_{\text{relay}(t2)}, \ldots, P_{\text{relay}(\text{tn})}$ are the sampled values of power in relay place. The cable and fault resistances being unknown, to find the cable power consumption during the fault, the LS method is formulated to find P_{cable}. Then, (10) can be written as

$$[k][x] = [m] \tag{13}$$

$$[k] = \begin{bmatrix} n & \sum_1^n I_{\text{fault}_i} & \sum_1^n I_{\text{fault}_i}^2 \\ \sum_1^n I_{\text{fault}_i} & \sum_1^n I_{\text{fault}_i}^2 & \sum_1^n I_{\text{fault}_i}^3 \\ \sum_1^n I_{\text{fault}_i}^2 & \sum_1^n I_{\text{fault}_i}^3 & \sum_1^n I_{\text{fault}_i}^4 \end{bmatrix}$$

$$[m] = \begin{bmatrix} \sum_1^n P_{\text{relay}} \\ \sum_1^n P_{\text{relay}} I_{\text{fault}_i} \\ \sum_1^n P_{\text{relay}} I_{\text{fault}_i}^2 \end{bmatrix} \tag{14}$$

[x] is the column matrix of the unknowns *A*, *B*, and *C*. Therefore, the value of the *[x]*, and then P_{cable} calculated by

$$[x] = [k]^{-1}[m]. \tag{15}$$

Therefore, the value of the fault resistance, with high accuracy, can be calculated by

$$R_{\text{fault}} = \frac{P_{\text{fault}}}{I_{\text{fault}}^2}. \tag{16}$$

B. Proposed Relay Settings Method

The proposed relay should be installed in the mainline. For instance, in Fig. 2, the relay should be installed at the Bus A. Also, a prefault setting is essential for the majority of relays, such as overcurrent and distance. Therefore, each relay needs a fault analysis to adjust the settings of the relay before the fault. In the proposed protection method, the settings are the relation of fault resistance to the slope of fault current rising. Before the fault, a $\Delta I/\Delta t$–R curve is calculated based on the different locations of the fault, as shown in Fig. 5. Thus, the slope of the fault current depends on fault resistance and Fig. 5 shows the behavior of this function. The reduction trend of this

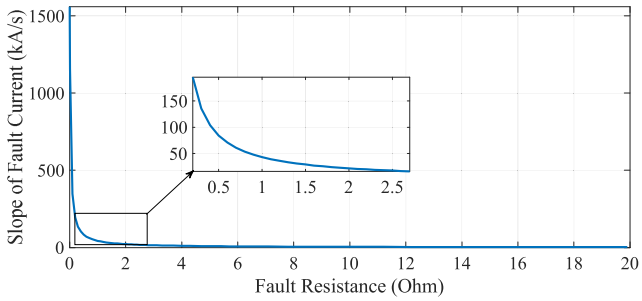

Fig. 5. Slope of fault current–fault resistance curve.

plot shows the reducing behavior of the slope of fault current against increasing the fault resistance or distance. Therefore, by increasing the distance of the fault location, the slope will be decreased. To design this figure, a prefault evaluation is needed for calculating the slope of fault current for each fault resistance, and hence, it will be a discrete plot. To calculate the slope of the fault current, continuous values of the fault resistance, a high accuracy plot fitting is essential. On the other hand, by increasing the number of samples, the accuracy of the plot and data fitting will be increased. In this article, the number of sampling data for resistance variation is 60 for fault resistance between 0 to 20 Ω, and the curve fitting is done by shape-preserving piecewise cubic interpolation. Therefore, the slope of fault current for different locations with different values can be defined. During the fault, based on the estimated fault resistance, the location of the fault will be estimated. Also, this method only needs calculating two curves for two CPLs, and then the slope changes for each distance can be calculated. For example, if the slope of fault current for CPL1 was 100 000 A/s and then for CPL2 was 80 000 A/s, and the distance between them was 100 m, the value of slope reduction will be 200 per meter.

Besides, this method can detect the fault in milliseconds by the mentioned curve. In the steady-state, the value of the slope is almost zero, because there is no variation in the current signal. However, during any disturbance, the slope of the current will be increased from zero to a higher value. Thus, a specific value of the slope of current can show the faulty situation in the system. The slope of the current can define this value of the threshold for the fault current with 20 Ω. In this system, the value of the threshold is 2334, which illustrates that after this slope, the fault occurs. The highest value selects the threshold for the fault resistance, which causes a fault current higher than 120% of the maximum normal current.

C. Operation of the Relay During the Fault

During the fault, the measurement device measures the values of current, voltage, and the slope of the fault current. Then, based on the proposed fault resistance estimation algorithm, the value of the fault resistance is estimated. Afterward, based on the slope-resistance curve, the location of the fault can be calculated. Then, the breaking signal will be sent to the C.B of the faulted CPL or line. The flowchart of the proposed method is shown in Fig. 6.

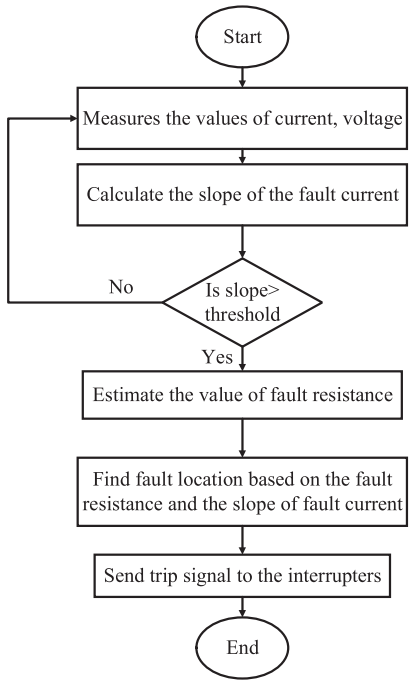

Fig. 6. Flowchart of the proposed method.

TABLE II
ESTIMATION OF FAULT RESISTANCE FOR DIFFERENT LOCATIONS OF FAULTS

Location	Actual fault resistance (Ω)	Estimated fault resistance (Ω)	Error (%)
CPL1	0.0100	0.0100	0.00%
CPL1	0.2000	0.2000	0.00%
CPL1	1.0000	0.9964	0.36%
CPL2	0.8000	0.7865	1.68%
CPL2	2.0000	1.9871	0.64%
CPL2	6.0000	5.9939	0.10%
CPL3	1.0000	0.9828	1.71%
CPL3	2.0000	1.9837	0.81%
CPL3	9.4000	9.3940	0.06%

V. SIMULATION RESULTS

A 220 V dc microgrid test system is considered to simulate the proposed protection strategy in DigSilent PowerFactory software environment by applying faults in different situations (see Fig. 7). The proposed approach is tested for different fault resistance values and locations, and the results are presented.

A. Performance Evaluation for Fault Resistance Estimation

Several faults with an unknown fault resistance are created at the time of $t = 1$ s in CPL1, CPL2, and CPL3. The length of cable between the main bus and CPL1, CPL2, and CPL3 are 60, 160, and 260 m, respectively. The current and voltage signals are measured using measurement devices installed in the relay place. In the case of estimation of fault resistance, the proposed strategy uses the predescribed power-sharing method, and the values of the estimated fault resistance are presented in Table II. Based on Table II, by increasing the value of the fault resistance, the error value increases; however, it still is in

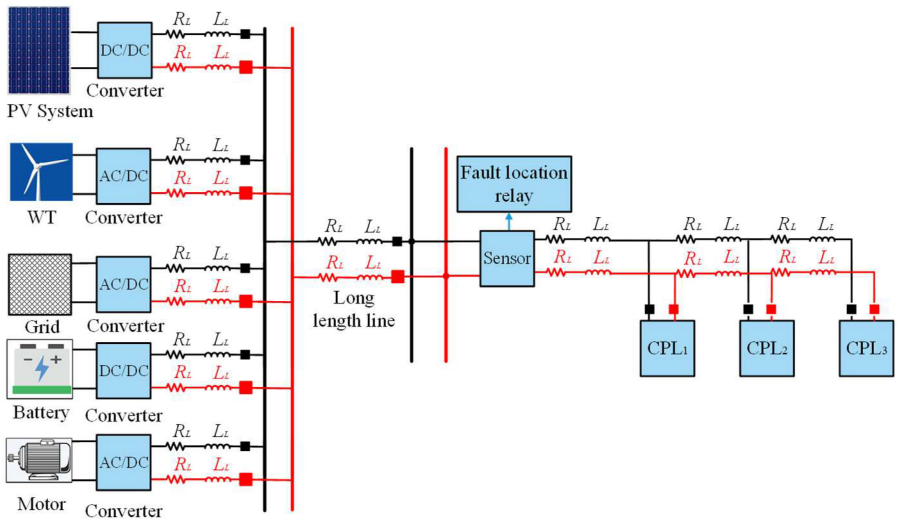

Fig. 7. Test microgrid system.

TABLE III
ESTIMATION OF FAULT RESISTANCE CONSIDERING UNCERTAINTIES

Location	Power of CPL	Fault resistance (Ω)	Error (%)
CPL1	+10%	0.2000	1.35%
CPL1	-10%	1.0000	3.08%
CPL2	+15%	0.8000	3.61%
CPL2	-15%	2.0000	4.01%
CPL3	+20%	1.0000	6.06%
CPL3	-20%	2.0000	6.63%

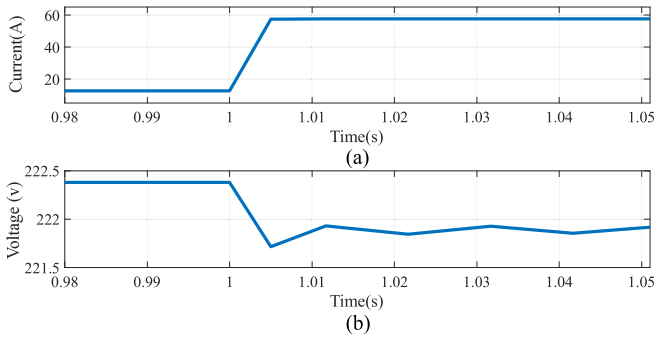

Fig. 8. Fault is occurred at $t = 1$ s. (a) Fault current. (b) Voltage waveform.

an acceptable range. Based on Table II, due to increasing of the length of cable, for the same values of the fault resistance for CPL1 and CPL3, namely 1 Ω, the estimation error of CPL 3 is more than CPL1.

The proposed method uses the power consumption of the CPLs. Hence, due to the consideration of uncertainties, the fault current is estimated for different values of the CPLs. In this case, the values of CPLs are assumed to be in the range of $\pm 20\%$ above/below the nominal power. The actual and estimated values of fault resistance are presented in Table III, considering uncertainties. By changing the power of CPLs, which can be realized by comparing Tables I and II, the error is increased by considering these uncertainties. But, it is still in an acceptable range and less than 6.63%.

B. Relay Settings

The settings of the proposed relay can be designed using the slope of the fault current. For instance, during a 3 Ω fault in CPL3, the current and voltage waveforms are shown in Fig. 8. The fault occurs in the $t = 1$ s. Hence, the first slope of the current can be calculated by $\Delta I/\Delta t$ from the fault occurrence time and the next one millisecond. Then, the slope-fault resistance curve can be designed for all CPLs and different fault resistances. In Fig. 9, the mentioned curve is designed for the case study. Fig. 9 shows the value of the slope of fault current for fault resistance between 0–20 Ω. It can be observed that increasing the value of fault resistance reduces the distance between curves. Therefore, locating HIFs requires more accuracy in measuring values, however during low resistance faults, the difference between curves is more, and error of fault locating becomes less.

Besides, for accurate locating of the fault in the line, the proposed method can calculate the exact value of the distance of the fault location from the relay. For example, for a fault resistance of 0.2 Ω, the values of slope for CPL1 and CPL3 are 194899 and 162558 A/s, respectively, and the distance between these CPLs is 200 m. Hence, the difference between the slopes is 32341 A/s. Therefore, the slope reduction is 161.705 A/s for each meter. For instance, if the measured slope is 191665 A/s, the fault location is 80 m. Moreover, the threshold of slope for fault detection is 20 Ω resistance. In this system, this value is 2334. Therefore, if the slope becomes more than 2334, the relay observes this situation as a faulty situation.

C. Robustness Against Disturbances

In a dc microgrid, some equipment can make an overvoltage or an inrush current, which can be wrongly detected as a

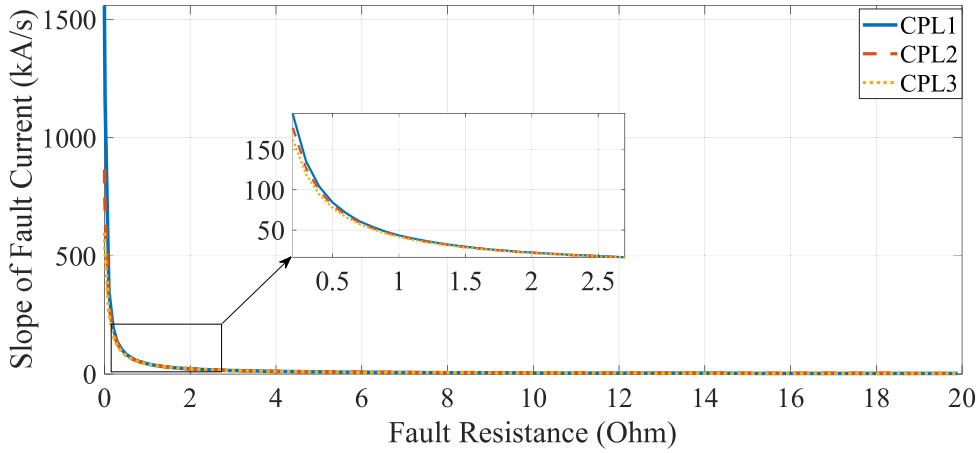

Fig. 9. Slope of fault current for fault resistance between 0 and 20 Ω.

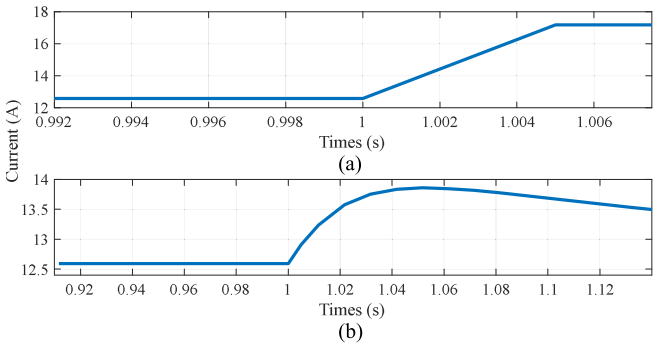

Fig. 10. Transient current for (a) switching event (b) capacitance discharge of motor.

TABLE IV
CALCULATED FAULT DISTANCE IN DIFFERENT FAULT LOCATIONS AND RESISTANCES

Faulty component	Estimated fault location (m)	Actual fault resistance (Ω)	Actual fault location (m)	Error of fault location (%)
CPL	159.98	0.010	160	0.00%
Line	102.20	0.200	100	2.20%
Line	198.67	0.500	200	0.66%
CPL	256.96	0.900	260	1.16%
CPL	56.57	1.200	60	5.71%
Line	57.11	1.00	60	4.81%

fault by relays. One of these disturbance resources is switching during the load increment, in which an overcurrent can flow in the main distribution line. However, the value of the slope of switching current is less than the slope of fault current, as illustrated in Fig. 10(a). If another CPL is connected to the system immediately, the current will be raised, and the slope of the current will be around 900 A/s, which is much less than the threshold of the fault current. Also, another disturbance resource is capacitance discharge of other components in the system. As shown in Fig. 10(b), the current will be raised after discharging the capacitor of other components such as motor, and the slope of this current is less than the threshold. Hence, these disturbance resources cannot impact on the proposed protection strategy.

D. Fault Location

A fault is simulated for various locations in the study system shown in Fig. 7 with different and fault resistances. The fault locations estimated by the proposed method are given in Table IV. It should be noted that due to the reduction of the fault current and power consumption of fault resistance, the accuracy of the proposed method is decreased by increasing the value of fault resistance; however, this error remains in an acceptable range. Also, an essential part of this article is evaluating the impact of CPLs on the fault current protection. Therefore, the proposed method considers a system with high penetration of CPLs. As presented in Table IV, since the algorithm is implemented in a dc microgrid, the fault distance is accurately calculated with at least a 95% confidence level by only implementing one local protection relay. Also, by increasing the distance, and the value of fault resistance, the error of the proposed method will be increased. However, the error is still in an acceptable range. Moreover, due to the usage of a threshold for fault detection, the fault detection method can detect the fault immediately. Besides, because the fault location algorithm is local and does not need any communication link, there is no delay in the proposed method. Hence, the location of the fault can be estimated in less than 10 ms. For instance, after the fault occurrence in dc microgrid, the current waveform of the relay is shown in Fig. 11. This fault is assumed as an unknown fault. The measured voltage and current values are 105.43 V and 1830 A, respectively. Therefore, using the proposed strategy, the estimated fault resistance is 0.01001 Ω. Also, the measured slope of the fault current is 366 000 A/s. Then, by using the fault location method, the estimated location is 160.018 m from the relay. Table IV gives information on the results of the proposed method in the several fault locations in both CPLs and lines.

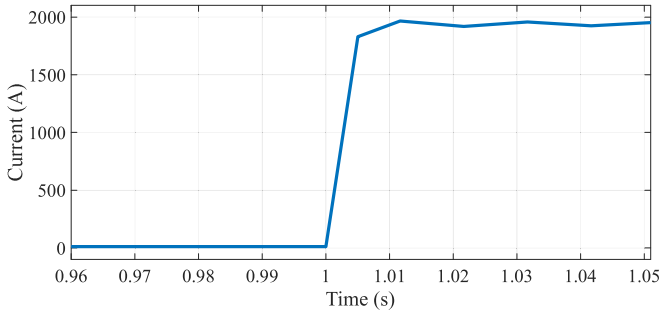

Fig. 11. Fault current waveform.

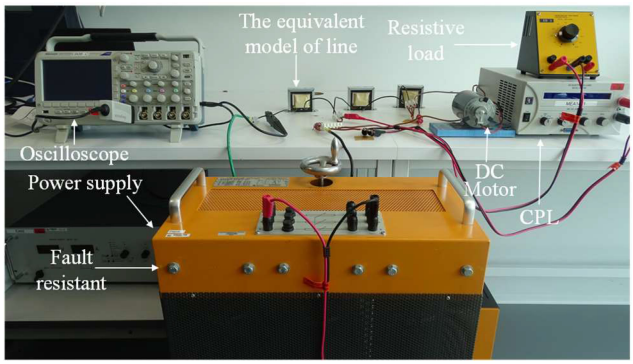

Fig. 12. Experimental setup for CPL protection method.

VI. Experimental Test Results

The preliminary validation of the local CPL protection has been performed in an LVdc branch by using the experimental setup depicted in Fig. 12. This setup was designed to scale the main system during the fault with less voltage and current levels. The experimental laboratory setup emphasizes on the implementation of the proposed protection strategy on a radial line equipped by CPLs to locate and detect the fault.

In this setup, the dc bus is modeled by a dc voltage source supplying a CPL, a dc resistive load, and a dc motor. An equivalent resistance and inductance of 0.16 Ω and 10 mH are used for representing the resistance and inductance of the lines, at each one is assumed to be a 200 m line. A variable CPL with 20 W, a 6.6 W dc resistive load, and a 10 W dc motor are connected to the dc system, and the high power resistance is connected to a switch and ground for making a fault resistance. The input dc voltage source is 20 V, and the fault current is measured at one side of the system by a DPO 2024B with a sampling rate of 1.3 kHz. Also, the capacitor of the dc link is scaled with the high internal capacitor of the delta Elektronika SM 60–100 to provide the capacitor discharge during the fault. In summary, the parameters of the experimental setup are represented in Table V.

Fig. 13 shows the fault current of the main distribution line during the fault for a load fault with 11.9 Ω fault resistance. In this case, the fault occurs at $t = 1.6$ s, and the fault current is increased to the maximum value in 110 ms. Moreover, as can be seen in Fig. 13, the measured current as a small magnitude of noise.

TABLE V
Parameters of Experimental Setup

Component	Parameter
Line	Resistance= 0.8 Ω/km, Inductance= 50 mH/km
Power supply	Delta Elektronika SM 60-100
CPL	DC electronic load EA-EL 3160-60, set to 20 W
Motor	DC Motor 10 W
Load	6.6 W DC resistive load
Fault resistance	0 Ω – 20 Ω
Measurement device	DPO 2024B, sampling rate 1.3 kHz, Tektronix TCP0020 AC/DC Current Probe

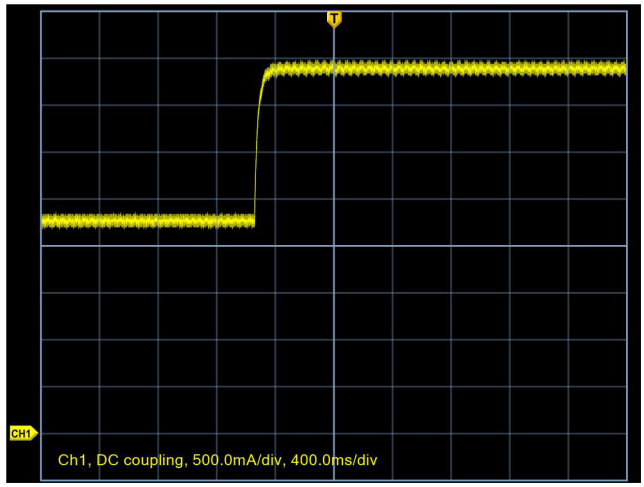

Fig. 13. Fault current of the main line during dc motor fault.

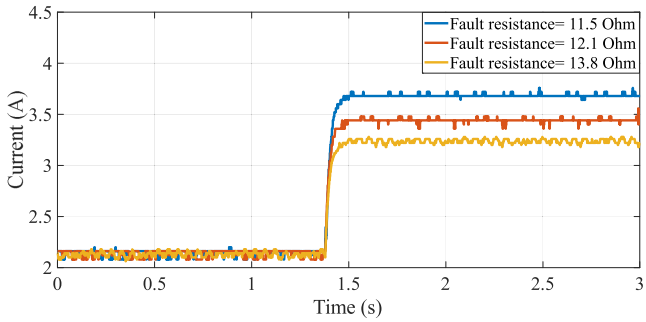

Fig. 14. Current for three different faults at CPL.

Therefore, due to the localized nature of the proposed method, the only source of noise is the noise of the measurement device, and there is no communication-related noise. As we discussed in Section III, at the first stage, the slope of the fault current-fault resistance curve is designed for the understudy setup. For calculating the accurate value of the threshold, as discussed before, the fault current by 120% more current magnitude than normal current is selected for determining the threshold value, which by increasing the fault resistance to 20 Ω, The threshold of fault current slope can be calculated for this setup at 28 A/s. Moreover, in Fig. 14, the fault currents for three different fault resistances

TABLE VI
EXPERIMENTAL FAULT LOCATION RESULTS OF THE PROPOSED METHOD

Faulty component	Actual fault resistance (Ω)	Fault location (m)	Calculated fault resistance (Ω)	Error (%)
DC Motor	19.84	600	19.04	4.04%
CPL	14.68	400	15.32	4.35%
DC load	15.21	200	14.68	3.48%
Line	12.63	200	12.47	1.26%
Faulty component	**Actual fault location (m)**	**Fault resistance (Ω)**	**Calculated fault location (m)**	**Error (%)**
CPL	600	9.76	581	3.07%
CPL	400	12.32	382	3.20%
Line	200	14.87	206	3.09%
Line	200	12.63	203	1.50%

by the recorded data are depicted. Based on this figure, by increasing the value of resistance of HIFs, the fault current for fault resistance of 11.5 Ω is 3.68 A, and it is decreased to 3.2 A for fault resistance of 13.8 Ω. Then, the difference between the fault and normal current decreases; thus, it increases the value of error in fault location algorithms. Therefore, the relay will start calculating the fault location for current with a current slope more than this threshold. Furthermore, as discussed in the results of simulation tests, increasing the fault resistance decreases the slope of fault current. The slope of fault current for fault with fault resistance of 11.5, 12.1, and 13.8 Ω are 35, 34.3, and 33.1 A/s, respectively. Thus, different faults occur in the setup at a different location and with different resistances. The values of errors are given in Table VI. In terms of fault resistance estimation, four different fault distances from the relay are tested, dc motor with 600 m, CPL with 400 m, dc load with 200 m, and line with 200 m. As expected, by increasing the actual fault resistance, the value of error will increase to approximately 4%. On the other hand, in terms of fault location estimation, during a fault at CPL with 12.32 Ω, the maximum error will be 3.2%. As can be seen from Table VI, although the fault resistance of a fault in line at the location of 200 m is higher than a fault in CPL at the location of 400 m, the error of line fault is lower than CPL fault. There are two reasons for this, first, the higher distance of CPL fault, and second the INR-based behavior of CPL during the fault. However, the proposed method accurately locates the CPL fault during HIFs.

In addition to the simulation results, the experimental fault location calculation results prove the effectiveness, accuracy, and authenticity of the proposed method for CPL protection in different cases. Also, the impacts of other loads such as dc motor, resistive load, and the CPL are evaluated in this scaled laboratory test, and the proposed method calculates the accurate place of fault efficiently and reliably.

VII. DISCUSSIONS AND COMPARISON

In the proposed protection strategy, the transient behavior of the fault current at the main distribution line was evaluated to calculate the value of the fault resistance and the location of the fault in the system with high penetration of CPLs. It is observed that the fault resistance is calculated using a power-sharing method, and the error of the value is in an acceptable range. On the other hand, due to the change of the behavior of the fault current characteristics by installing CPLs, this technique considers the impact of CPLs on fault location method. This feature clearly distinguishes this method for the protection of dc microgrids. In the case of the fault with high resistance, due to the decrement of the fault current, the error of the method is increased to over 1%. Also, due to calculating a threshold for fault detection, the protection method detects the fault immediately after beginning the current rising.

The proposed method was also implemented on a dc microgrid with a high penetration of CPLs. The most prominent feature of the proposed method is that it uses one relay and the related measured values in one line. Therefore, implementing a localized relay instead of several relays reduces cost and uses transient behavior of the system, which can increase the operation time of the method. The flowchart of the proposed technique shown in Fig. 6 was presented considering the threshold of fault detection. In the threshold calculation, the other disturbances were considered so that it guaranteed that the protection method detects the faults immediately. Also, the fault estimation method was used, and results prove the high accuracy of calculated fault resistances.

This method also protects the lines and CPLs. Based on the fault current in the dc microgrid shown in Fig. 11, we find that the slope of rising is the key factor of the proposed protection strategy. In this article, the error of the fault location for fault resistance less than 1 Ω is almost 2.0%, which is highly suitable for protection strategies. Also, as presented in Table II, the error of the fault resistance estimation for different values of fault resistance and fault location is less than 0.2%. This is the first stage of fault protection. Thus, it can reduce the error of the protection strategy and can be implemented with other methods. Additionally, the uncertainty in the variation of power of CPLs was taken into account, and it revealed that the error of the fault resistance estimation is still in an acceptable range.

To verify the proposed technique for the protection of dc microgrids with high penetration of CPLs, experimental tests were conducted. As shown in Table VI, the fault resistance estimation method has a maximum 4.35% error for different locations in the system and also a maximum 3.20% error for calculating the location of the fault in the system. In these tests, the fault resistances were assumed to be a high value to show the effectiveness of the proposed method on the HIFs.

Moreover, the effectiveness of the proposed method is compared in terms of cost, communication link, error, considering the HIFs, etc., with other existed researches. It should be noted that due to the lack of study on the protection of CPLs, this method is compared with other component protection methods, which is presented in Table VII. In [13], a fault location scheme for the PV systems is presented, which, due to the lack of communication links, the cost of this method is low. The maximum value of error is almost 8%, and the HIF cases not considered in this article. In [20], the suggested method uses the circuit analyses during fault; however, during different operational conditions, the error of fault location increases to 24%. The fault location methods in [14]–[21] using

TABLE VII
COMPARING OF THE PROPOSED METHOD WITH OTHER METHODS

Method	Cost	Communication link	Fault resistance estimation function	Required sampling rate	Load behavior	Line length	Error	HIF	Maximum fault resistance	Fault detection possibility
[13]	Low	Not Required	No	20 kHz	Not considered	Low length lines	8%	Not considered	500 mΩ	No
[14]	High	Required	Yes	50 kHz	Not considered	High length lines	8%	Not considered	5 Ω	No
[20]	Low	Not Required	No	5 kHz	Not considered	Medium length lines	24%	Considered	10 Ω	Yes
[21]	High	Not Required	No	1 kHz	Not considered	Low length lines	16%	Not Considered	20 mΩ	No
[22]	High	Not Required	No	780 Hz	Not considered	Medium length lines	6%	Not Considered	0.1 Ω	Yes
[23]	High	Required	No	200 kHz	Not considered	High length lines	2.4 %	Considered	100 Ω	No
[24]	Low	Required	No	750 kHz	Not considered	High length lines	3%	Considered	20 Ω	No
[25]	High	Required	No	10 kHz	Not considered	Low length lines	1%	Not considered	0 Ω	Yes
[26]	High	Required	Yes	20 kHz	Considered	Medium length lines	14%	Considered	15 Ω	No
[27]	High	Required	Yes	100 kHz	Considered	Medium length lines	5%	Considered	20 Ω	No
Proposed Method	Low	Not Required	Yes	1.3 kHz	Considered	Medium length lines	4%	Considered	20 Ω	No

communication infrastructure, and it increases the cost; however, Kumar and Saxena [24] eliminates the communication links in the presented scheme, but the error of fault location rises to 16%. The methods mentioned in [22] and [23] use traveling wave transients, and they are local and communication-based fault location schemes, respectively. However, these methods require a current injection device, accurate transient current sensor, and fast time difference unit, which due to the requiring additional equipment, the cost of these methods is high. Moreover, in addition to the equipment of the fault location method in [22] and [23] requires communication link infrastructure.

Furthermore, the high sampling frequency of [23] causes difficulties during the implementation of the sensor. The neural network-based fault location method of [26] required communication links, and also, this method did not consider the fault resistance and load behavior. An additional fault location module should be connected to the dc line in [26], and both ends of the line segment must be connected to a communication link. Thus, this method increases the total cost of the fault location scheme. Also, the high value of error reduces the efficiency of the protection method. The voltage-based fault location strategy of [27] requires a communication link and also measurement units with high sample rates.

On the other hand, generally, the proposed scheme can be compared with other existed methods in different terms. Due to the local structure of the proposed method, the cost and noise in this method are low, and also requires sensors with a low sampling rate. Besides, the HIFs are considered in this method for fault resistances up to 20 Ω with a maximum error of 4%, which is in an acceptable range.

VIII. CONCLUSION

In this article, an efficient and effective protection scheme for a dc microgrid with high penetration of CPLs was proposed. The behavior of the fault current was measured at the main distribution line and used to develop the protection method. By exploiting the localized measurements, there is no communication time delay involved, and moreover, the protection scheme robust against the disturbance, and other disturbance events cannot affect the proposed method. In this scheme, the first-order derivatives of fault current were utilized to locate and detect high- and low-resistance faults in the CPL line. The proposed protection strategy was applied to a test microgrid system for various locations of fault, such as line and CPL. The thresholds and settings of the protection scheme can be calculated analytically or practically before the fault in an offline manner to adjust the parameters of the relay. The proposed protection scheme is robust, fast, accurate, and considers the behavior of CPL in dc microgrids and locates the faults with the least possible error, which is easy to extend to other systems and configurations. A dc line with three different types of loads was considered for this article and implemented in a real scaled testbed. Finally, the performance of the proposed protection strategy was experimentally tested. The experimental tests showed that the proposed method has a maximum 3.2% error for fault locating scheme in the practical situation, and in this way, the proposed scheme was validated.

REFERENCES

[1] M. F. Zia, E. Elbouchikhi, and M. Benbouzid, "Optimal operational planning of scalable DC microgrid with demand response, islanding, and battery degradation cost considerations," *Appl. Energy*, vol. 237, pp. 695–707, 2019.

[2] H. R. Baghaee, M. Mirsalim, G. B. Gharehpetian, and H. A. Talebi, "A decentralized power management and sliding mode control strategy for hybrid AC/DC microgrids including renewable energy resources," *IEEE Trans. Ind. Informat.*, to be published, doi: 10.1109/TII.2017.2677943.

[3] S. Zhikang *et al.*, "Hierarchical structure and bus voltage control of DC microgrid," *Renewable Sustain. Energy Rev.*, vol. 82, pp. 3670–3682, Feb. 2018.

[4] K. A. Saleh, A. Hooshyar, and E. F. El-Saadany, "Hybrid passive-overcurrent relay for detection of faults in low-voltage DC grids," *IEEE Trans. Smart Grid*, vol. 8. no. 3, pp. 1129–1138, May 2017.
[5] H. S. Amir *et al.*, "An overview of microgrid protection methods and the factors involved," *Renewable Sustain. Energy Rev.*, vol. 64, pp. 174–186, Oct. 2016.
[6] S. D. A. Fletcher, P. J. Norman, K. Fong, S. J. Galloway, and G. M. Burt, "High-speed differential protection for smart DC distribution systems," *IEEE Trans. Smart Grid*, vol. 5. no. 5, pp. 2610–2617, Sep. 2014.
[7] D. D. Patil and S. Bindu, "Real-time protection technique for DC microgrid using local measurements," in *Proc. Technol. Smart-City Energy Secur. Power*, 2018, pp. 1–6.
[8] N. Bottrell, M. Prodanovic, and T. C. Green, "Dynamic stability of a microgrid with an active load," *IEEE Trans. Power Electron.*, vol. 28, no. 11, pp. 5107–5119, Nov. 2013.
[9] G. Sulligoi, D. Bosich, G. Giadrossi, L. Zhu, M. Cupelli, and A. Monti, "Multi-converter medium voltage DC power systems on ships: Constant-power loads instability solution using linearization via state feedback control," *IEEE Trans. Smart Grid*, vol. 5, no. 5, pp. 2543–2552, Sep. 2014.
[10] SELCO foundation, "Neelakantarayanagaddi village microgrid," 2015, Accessed: Apr. 17, 2017. [Online]. Available: http://microgridprojects.com/microgrid/neelakantarayanagaddi-villagemicrogrid/
[11] D. Snehamoy, R. K. Patnaik, and P. K. Dash, "Fault detection and location of photovoltaic based DC microgrid using differential protection strategy," *IEEE Trans. Smart Grid*, vol. 9, no. 5, pp. 4303–4312, Sep. 2018.
[12] S. Azizi, M. Sanaye-Pasand, M. Abedini, and A. Hasani, "A traveling-wave-based methodology for wide-area fault location in multiterminal DC systems," *IEEE Trans. Power Del.*, vol. 29, no. 6, pp. 2552–2560, Dec. 2014.
[13] I. M. Karmacharya and R. Gokaraju, "Fault location in ungrounded photovoltaic system using wavelets and ANN," *IEEE Trans. Power Del.*, vol. 33, no. 2, pp. 549–559, Apr. 2018.
[14] S. Jiang, C. Fan, N. Huang, Y. Zhu, and M. He, "A fault location method for DC lines connected with DAB terminal in power electronic transformer," *IEEE Trans. Power Del.*, vol. 34, no. 1, pp. 301–311, Aug. 30, 2018.
[15] Q. Cui and Y. Weng, "Enhance high impedance fault detection and location accuracy via μ-PMUs," *IEEE Trans. Smart Grid*, vol. 11, no. 1, pp. 797–809, Jan. 2020.
[16] B. Hoseinzadeh, M. H. Amini, C. L. Bak, and F. Blaabierg, "High impedance DC fault detection and localization in HVDC transmission lines using harmonic analysis," in *Proc. IEEE Int. Conf. Environ. Elect. Eng. IEEE Ind. Commercial Power Syst. Europe*, 2018, pp. 1–4.
[17] X. Lin *et al.*, "Regional protection scheme designed for low-voltage micro-grids," *Int. J. Elect. Power Energy Syst.*, vol. 64, pp. 526–535, 2015.
[18] R. Mohanty and A.K. Pradhan, "A superimposed current based unit protection scheme for dc microgrid," *IEEE Trans. Smart Grid*, vol. 9, no. 4, pp. 3917–3919, Jul. 2018.
[19] H. J. Laaksonen, "Protection principles for future microgrids," *IEEE Trans. Power Electron.*, vol. 25, no. 12, pp. 2910–2918, Dec. 2010.
[20] J. Yang, J. E. Fletcher, and J. O'Reilly, "Multiterminal DC wind farm collection grid internal fault analysis and protection design," *IEEE Trans. Power Del.*, vol. 25, no. 4, pp. 2308–2318, Oct. 2010.
[21] E. Christopher, M. Sumner, D. W. P. Thomas, X. Wang and F. de Wildt, "Fault location in a zonal DC marine power system using active impedance estimation," *IEEE Trans. Ind. Appl.*, vol. 49, no. 2, pp. 860–865, Mar./Apr. 2013.
[22] J. D. Park, J. Candelaria, L. Ma, and K. Dunn, "DC ring-bus microgrid fault protection and identification of fault location," *IEEE Trans. Power Del.*, vol. 28, no. 4, pp. 2574–2584, Oct. 2013
[23] Q. Lin, G. Luo, and J. He, "Travelling-wave-based method for fault location in multi-terminal DC networks," *J. Eng.*, vol. 2017, no. 13, pp. 2314–2318, 2017.
[24] R. Kumar and D. Saxena, "Fault location in multilateral distribution network with electric vehicle charging load," *Energy Storage*, vol. 1, no. 5, Oct. 2019, Art. no. e85.
[25] A. Abdali, K. Mazlumi, and R. Noroozian, "High-speed fault detection and location in DC microgrids systems using Multi-Criterion System and neural network," *Appl. Soft Comput.*, vol. 79, pp. 341–53, Jun. 1, 2019.
[26] Y. Yang, C. Huang, and Q. Xu, "A fault location method suitable for low-voltage DC line," *IEEE Trans. Power Del.*, vol. 35, no. 1, pp. 194–204, Feb. 2020.
[27] K. Jia, M. Li, T. Bi, and Q. Yang, "A voltage resonance-based single-ended online fault location algorithm for DC distribution networks," *Sci. China Technol. Sci.*, vol. 59, no. 5, pp. 721–729, May 1, 2016.
[28] N. Bayati, A. Hajizadeh, and M.N. Soltani, "Protection in DC Microgrids: A comparative review," *IET Smart Grid*, vol. 1, no. 3, pp. 66–75, Oct. 2018.
[29] J. Yang, J. E. Fletcher, and J. O'Reilly, "Short-circuit and ground fault analyses and location in VSC-based DC network cables," *IEEE Trans. Ind. Electron.*, vol. 59, no. 10, pp. 3827–3837, Oct. 2012.